Use of S-wave attenuation from perforation shots to map the growth of the stimulated reservoir volume in the Marcellus gas shale

Yunhui Tan[1], Chengping Chai[1], and Terry Engelder[1]

Abstract

Water-filled fractures stimulated by hydraulic fracturing will severely attenuate S-waves. By comparing the P- and S-wave amplitudes generated from perforation shots in the Marcellus gas shale, one can infer the existence and constrain the location of stimulated hydraulic fractures. The waveforms of the perforation shots in unstimulated gas shale are first analyzed to define the prestimulation radiation pattern. Then the change of perforation-shot S-wave waveform is examined for information about the development of hydraulic fractures. S-wave attenuation validates the existence of offstage hydraulic fractures and the invasion of treatment fluid from another neighbor stage. This method might have potential use in designing an active seismic survey to more effectively monitor hydraulic-fracture stimulation beyond the current microseismic mapping techniques.

Introduction

The combination of hydraulic fracturing and horizontal drilling is key to the economic development of unconventional gas shale. So far, microseismic monitoring remains the most effective technique to visualize the growth of the stimulated reservoir volume (SRV) in the spatial and time domains (Maxwell, 2010; Maxwell and Cipolla, 2011). Locations of microseismic events as well as other information (e.g., focal mechanism, b value) have been used to help understand the stimulation process (Eisner et al., 2010b; Kendall et al., 2011). However, microseismic monitoring of the stimulation is often hampered by the problem of distinguishing between induced events and triggered events.

Induced (or wet) microseismic events are those associated with opening and slip of fractures caused by the stimulation fluid. Triggered (or dry) microseismic events are driven by the change in stress field associated with the induced strain within and surrounding the zone of stimulated fractures. Triggered events can give a false sense of the size of the stimulated reservoir volume. On the contrary, the presence of the treatment fluid is direct evidence for fractures interconnected with the wellbore, hence the actual SRV.

Another challenge of microseismic monitoring is the uncertainty in hypocentral locations for induced and triggered events, and this further complicates identification of the SRV (Eisner et al., 2009). Perforation shots during the completion process of a lateral have well-defined locations and initiation times; hence, there is much less uncertainty about the hypocentral location.

It is well known that S-waves are not transmitted by fluid. The effect in laboratory experiments is the large attenuation of S-waves in cracked, saturated rock (Toksöz et al., 1979; Johnston and Toksöz, 1980). Taking advantage of this property, water-filled open fractures were identified in a hot dry rock (HDR) geothermal reservoir (Fehler, 1982; Fehler and Pearson, 1984). Here we apply the same method to our microseismic data set of a hydraulic-fracture stimulation of the Marcellus gas shale in Washington County, Pennsylvania.

The configuration of the experiment includes four laterals (3H, 4H, 10H, and 11H) that were stimulated using a zipper-fracture sequence (Figure 1). Two microseismic arrays were installed to monitor the completion. One three-component array with eight accelerometers was deployed in the 2H lateral and was moved to three locations to be closer to the stages being fractured. An array was also deployed on the surface. These two arrays were operated by two service companies; hence, the receiver times were not synchronized.

We selected the perforation-shot waveforms gathered from the downhole array for this study. The downhole microseismic raypaths traveled completely within the reservoir, which provided the simplest possible configuration for observing the developing SRV during this experiment. Hypocenters mapped from surface arrays were used to define the location of stimulated fractures as the experiment proceeded. Relative to downhole data, surface microseismic data reduce uncertainty in the horizontal location of hypocenters in the Marcellus layer (Eisner et al., 2010a).

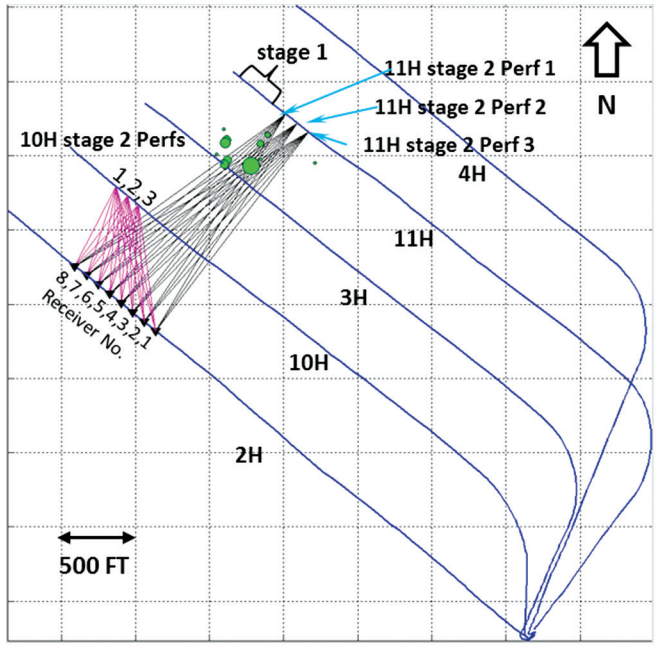

Figure 1. Map view of wells and microseismic events (green dots) from 11H Stage 1. Raypaths of 10H Stage 2 (cyan lines) and 11H Stage 2 (black lines) were also plotted. Black triangles represent receivers. The size of the dots is proportional to the magnitude of events as determined from a surface array.

[1]Pennsylvania State University.

http://dx.doi.org/10.1190/tle33101090.1

Waveforms of perforation shots in the unstimulated Marcellus Shale

Case 1 (10H Stage 2 perforations 1 through 3). Three perforations were shot during Stage 2 of the 10H lateral after stimulation of the first two stages (3H Stage 1 and 10H Stage 1) on this pad. The raypaths from these three perforations to the receivers in the 2H lateral are mapped by the cyan lines in Figure 1. The volume through which the rays passed was unstimulated at the time of the perforation shots. Therefore, we assume that the waveforms from these perforation shots represent wave propagation in undisturbed Marcellus gas shale. There are clear P-wave, SH-wave, and SV-wave phases in the waveform (Figure 2). The large P/S amplitude ratio is consistent with perforation shots rather than rock-on-rock slip events.

A perforation shot can be treated as an increase of the borehole surface area. The radiation pattern then can be calculated using equation 8 of Fehler and Pearson (1984) as

$$A_{\mathrm{P}}(\varnothing, R) = \frac{K_{\mathrm{P}}}{R}\left[(\lambda+\mu) - \mu\cos^2(\varnothing)\right]\exp\left(-\frac{\pi f R}{Q_{\mathrm{P}} V_{\mathrm{P}}}\right). \quad (1)$$

$$A_{\mathrm{S}}(\varnothing, R) = \frac{K_{\mathrm{S}}}{R}(\sin\varnothing\cos\varnothing)\exp\left(-\frac{\pi f R}{Q_{\mathrm{S}} V_{\mathrm{S}}}\right). \quad (2)$$

In these equations, A_{P} and A_{S} are the P- and S-wave amplitudes, $\varnothing$ is the angle between borehole axis and ray-propagation direction, R is the distance between source and receiver, f is the dominant frequency of the wave, and λ and μ are the two Lamé parameters. See the original source for an in-depth discussion of these two equations (Fehler and Pearson, 1984).

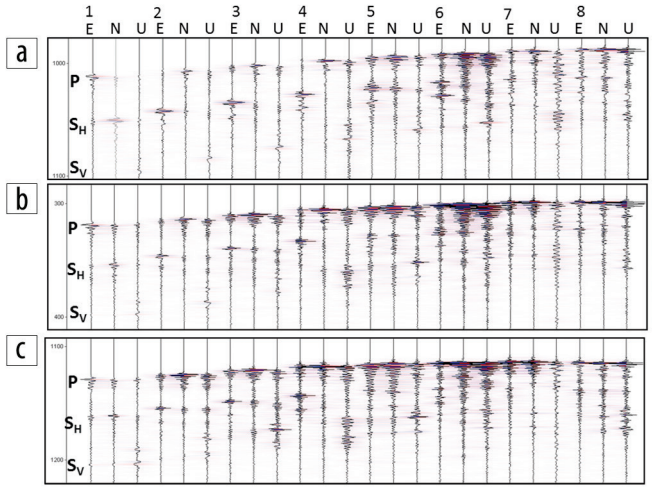

Figure 2. Waveforms of the 10H Stage 2 perforation shots, A-Perf 1, B-Perf 2, C-Perf 3. The three components of each receiver were grouped together. The three components were rotated to the east, north, and up directions (E, N, U). The vertical axis is time (in milliseconds) from an arbitrary origin time. The scale of the waveforms is adjusted for best visualization.

According to the Fehler-Pearson equations, the radiation pattern exhibits the largest S-wave amplitude at $\varnothing = 45°$.

However, even when Ø = 5° or 85°, S-wave amplitude is still about 20% of the amplitude at Ø = 45°. Hence, they should still be visible from most orientations unless attenuated by other factors.

We picked the maximum amplitudes of the P- and SH-waves from each trace, corrected by the radiation pattern, and then plotted them against $1/R$ to correct for the effects of geometric spreading (Figure 3). During the calculation, we assumed $\lambda = \mu$. Because the perforations and receivers are close (i.e., on the order of a few wavelengths), the attenuation effect of the medium can be ignored. The corrected equation is shown below:

$$A_P(Ø, R)/(2 - \cos^2(Ø)) = K_P \mu \frac{1}{R}. \quad (3)$$

$$A_S(Ø, R)/(\sin Ø \cos Ø) = K_S \frac{1}{R}. \quad (4)$$

The corrected amplitude is a linear function of the inverse of the distance between source and receiver. The slopes are $K_P\mu$ and K_S for the P-wave and S-wave, respectively, which are related only to the perforation yield itself and the rock property immediately around the perforation. These data fall around a straight line (Figure 3). However, the intercept of the best-fit line of the P-wave data is not zero (Figure 3a). This is probably because the elastic properties of the shale were not perfectly known. The intercept of the best-fit line for the S-wave data is closer to zero (Figure 3b). This is because unlike the P-wave, the radiation pattern of the S-wave does not depend on the elastic properties of the rock (equation 2). However, this confirms that the radiation-pattern prediction (equations 1 and 2) is correct.

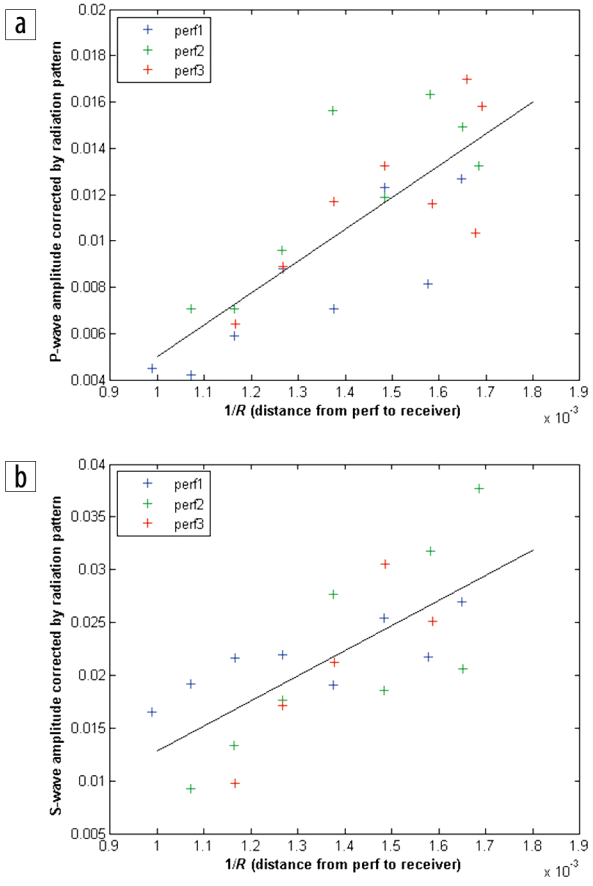

Figure 3. Plot of the (a) P-wave and (b) S-wave amplitude for the 10H Stage 2 perforation shots with correction of radiation pattern. The horizontal axis is $1/R$ (inverse of the distance from the source to receiver) (unit in ft^{-1}). The vertical axis is amplitude divided by radiation pattern (equations 3 and 4). The best-fit linear function to part (a) is y = 13.71 × −0.0087; the corresponding coefficient of determination (R^2) is 0.647. The best-fit linear function to part (b) is y = 23.743 x −0.0109; the corresponding coefficient of determination (R^2) is 0.524.

Evidence of water-filled hydraulic fractures

Case 2 (3H Stage 3). The 3H Stage 2 was stimulated as the third stage in this experiment. The microseismic events detected by the surface array show two linear clusters, one near the stage and another offstage (Figure 4). Is the offstage lineament induced and thus a hydraulically opened fracture or a series of triggered events responding to nearby rock strain?

Here we use two perforation shots from 3H Stage 3 which are near the offstage microseismic lineament. The time between the end of fracking Stage 2 and perforation of Stage 3 is about two hours. The P-waveforms of two perforations are identical, whereas the S-waves are dramatically different (Figure 5). Despite the fact that the P-wave amplitudes are about the same for the two perforations, the S-wave amplitudes of perforation shot 3 are only about a quarter of those of perforation shot 1.

The range of the ray angle Ø is about the same for the two perforation shots. Because the radiation pattern cannot be the main factor that caused these differences, we conclude that

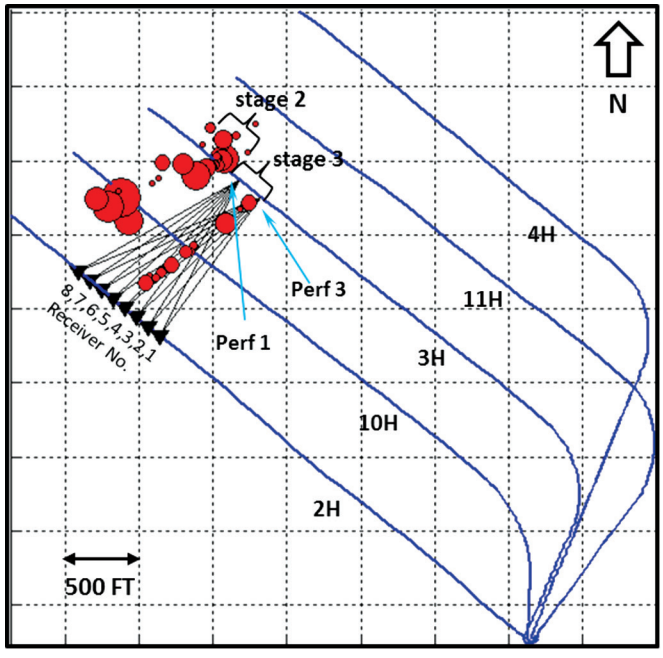

Figure 4. Map view of wells and microseismic events (red dots) of 3H Stage 3. The size of the circles is proportional to the microseismic event magnitude. Black triangles represent receivers. The size of the dots is proportional to the magnitude of events.

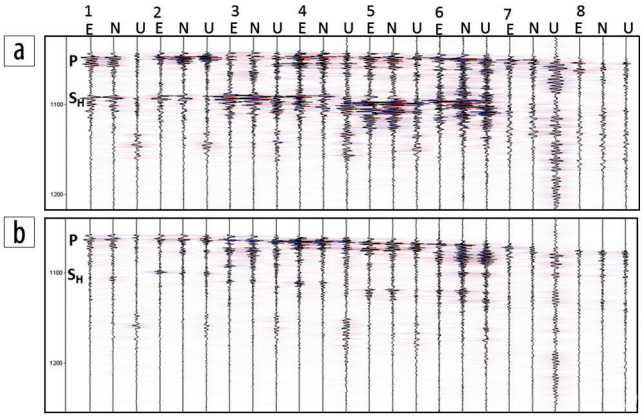

Figure 5. Waveform of 3H Stage 3 perforation shots, A-Perf shot 1, B-Perf shot 3. Notice that the SH-waveform is much smaller (i.e., attenuated) from perf shot 3 relative to the waveform from perf 1. The three components were rotated to the east, north, and up directions (E, N, U). The vertical axis is time (in milliseconds) from an arbitrary origin time. The scale of the waveforms is adjusted for best visualization.

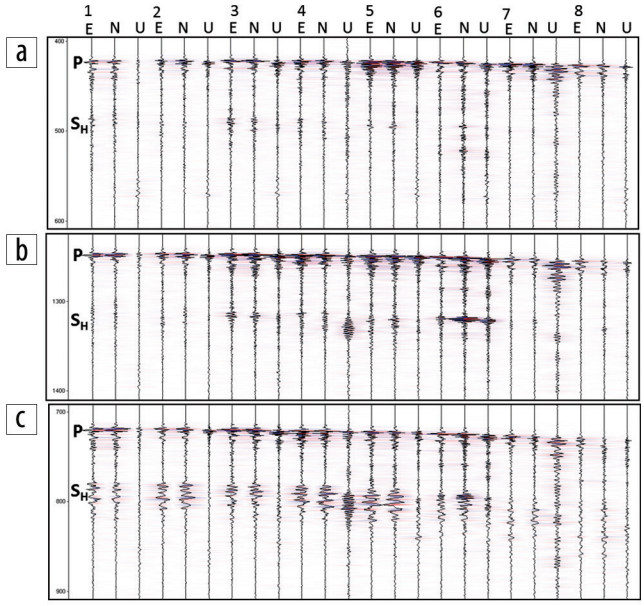

Figure 6. Waveform of 11H Stage 2 perforation shots, A-Perf shot 1, B-Perf shot 2, C-Perf shot 3. Notice that the SH-wave in perf shot 3 is much larger than those in perf shots 1 and 2. The three components were rotated to the east, north, and up directions (E, N, U). The vertical axis is time (in milliseconds) from an arbitrary origin time. The scale of the waveforms is adjusted for best visualization.

water-filled fractures are responsible for the offstage microseismic lineament. The closure time for hydraulic fractures in gas shale ranges from 700 hours to 3000 hours depending on the frack fluid, permeability and pressure of the shale, and so forth. Therefore, at the time of perforation, these fractures will remain open, and we will not be able to distinguish propped and unpropped fractures.

The fact that Traces 7 and 8 from perf shot 1 also have smaller S-wave magnitudes implies that there might be a water-filled fracture near geophones 7 and 8. This is confirmed by the same pattern from Traces 7 and 8 of perf shot 2.

In the map view, the raypaths of geophones 1 through 4 from perf shot 1 pass the linear cluster of offstage events as well (Figure 4), but the S-waves are still present in Figure 5a. This might be because the hydraulic fracture is above or below the raypaths. The S-wave attenuation method has a better constraint to the hydraulic fractures near the wellbore. During analysis of S-wave attenuation, we need to take the 3D geometry of the hydraulic fracture into consideration.

Case 3 (11H Stage 2). Stage 2 for 11H was perforated two hours after the stimulation of 11H Stage 1, which was the fourth stage of the stimulation sequence in this experiment. The microseismic event locations of 11H Stage 1 have "invaded" Stage 2 (Figure 2). We can validate this by comparing the three perforation shots of 11H Stage 3 (Figure 6). Perf shots 1 and 2 showed strong S-wave attenuation, whereas perf shot 3 did not. This might be because of the communication between Stage 1 and Stage 2. Some high-pressure water migrated sideways instead of propagating forward into the reservoir formation.

One interesting observation from perf shot 2 is that geophone 6 shows a strong S-wave signal. This demonstrates that stimulated fractures might be absent along its raypath. The hydraulic fracture is not continuous at this point. Another possibility is that proppant is packing or bridging at this point, which might result in the transmission of S-waves. However, if that is true, it means the section of fracture closer to the wellbore containing proppants will still attenuate S-waves strongly. Because the frequency of the perforations is relatively high, the Fresnel zone of these rays should be quite narrow. Thus the perforation S-wave attenuation is sensitive to the existence of water-filled hydraulic fractures.

Discussion

Radiation pattern of perforations. The Fehler-Pearson equations describing the radiation pattern do not predict change of amplitude in the surface perpendicular to the perforated borehole axis. In our experiment, the raypaths travel along a nearly horizontal plane. Therefore, the radiation pattern of perf shots should be consistent. However, there are some concerns about the symmetry of the perforation shots because the perf gun is not oriented consistently from one shot to the next (Leo Eisner, personal communication, 2014; Shawn Maxwell, personal communication, 2014). The symmetry depends on the type of perforation gun and the phase between the shaped charges. More research needs to be conducted by operators collaborating with service companies to understand the symmetry in the perforation radiation patterns.

Another argument about the radiation pattern is that if the pattern really emits a dipole body force, the P-wave amplitude should be at its maximum when S-wave amplitude is at its minimum. The fact that P-wave arrival amplitude is smaller when S-wave amplitude disappears suggests that they are both attenuated but that the S-wave was attenuated more. Thus we eliminate the possibility that these attenuations are all caused by the effects of radiation patterns instead of the existence of water-filled fractures.

Implication on hydraulic-fracture design and microseismic monitoring. This study shows that even with only a few observations, it is possible to constrain the location of hydraulic fractures (i.e., wet microseismic events) and the extent of the stimulated reservoir volume. Microseismic service companies might take advantage of this phenomenon to provide further constrains on the SRV in addition to the microseismic event clouds. One proposal is to install more receivers to expand ray coverage. Crosswell tomography is another possibility for accurately monitoring the hydraulic-fracturing process. When stimulation adds more open fractures in the reservoir, the array configuration needs to be carefully and cleverly moved to avoid the effects of preexisting hydraulic fractures.

P-wave attenuation might provide additional constraint on the location of hydraulic fractures. According to Fehler (1982), a water-filled unpropped open fracture 1 mm wide can attenuate the energy of incident P-waves by 60%. However, the transmission and reflection of P-waves through a viscous fluid layer changes with incident angle, which might complicate the interpretation of P-wave attenuation.

The strong attenuation of S-waves in the stimulated reservoir also raises concern about the effectiveness of the downhole microseismic-monitoring method. Ordinarily, we expect to see at least one order of magnitude more events recorded on the downhole array compared with the surface array because of geometric spreading. However, in this experiment, the number of events picked by the downhole array is about the same order of magnitude as the surface array. One explanation is that the strong S-wave attenuation causes an underestimation of the number of events and hence the SRV. This is possible considering that most of the energy released during microseismic events arises from shearing instead of opening motion between fracture walls, and most of the energy is carried by S-waves instead of P-waves.

Even if the event-detection algorithm focuses on P-waves, the strong attenuation might cause underestimation of the magnitude of the events. Therefore, the downhole microseismic survey design should be more effective if the microseismic rays do not pass through stimulated regions.

Another observation from this experiment is that offstage hydraulic-fracture propagation can be quite common. This raises concern about the quality of the casing cement along the wellbore. With higher-quality cement jobs that yield more efficient completions, the operators should increase their benefit/cost ratio.

Conclusions

Water-filled fractures (propped or not) in any rock volume strongly attenuate S-waves. Taking advantage of this property, we can constrain the locations of stimulated fractures by comparing the waveforms from neighboring perforation shots and correlating them with the microseismic event clusters. This phenomenon could be used in the design of active seismic experiments to detect hydraulic fractures as an independent measure of the SRV relative to microseismic monitoring. TLE

References

Eisner, L., P. M. Duncan, W. M. Heigl, and W. R. Keller, 2009, Uncertainties in passive seismic monitoring: The Leading Edge, **28**, no. 6, 648–655, http://dx.doi.org/10.1190/1.3148403.

Eisner, L., B. J. Hulsey, P. Duncan, D. Jurick, H. Werner, and W. Keller, 2010a, Comparison of surface and borehole locations of induced seismicity: Geophysical Prospecting, **58**, no. 5, 809–820, http://dx.doi.org/10.1111/j.1365-2478.2010.00867.x.

Eisner, L., S. Williams-Stroud, A. Hill, P. Duncan, and M. Thornton, 2010b, Beyond the dots in the box: Microseismicity-constrained fracture models for reservoir stimulation: The Leading Edge, **29**, no. 3, 326–333, http://dx.doi.org/10.1190/1.3353730.

Fehler, M., 1982, Interaction of seismic waves with a viscous liquid layer: Bulletin of the Seismological Society of America, **72**, no. 1, 55–72.

Fehler, M., and C. Pearson, 1984, Cross-hole seismic surveys: Applications for studying subsurface fracture systems at a hot dry rock geothermal site: Geophysics, **49**, no. 1, 37–45, http://dx.doi.org/10.1190/1.1441559.

Johnston, D. H., and M. N. Toksöz, 1980, Ultrasonic P and S wave attenuation in dry and saturated rocks under pressure: Journal of Geophysical Research: Solid Earth, **85**, no. B2, 925–936, http://dx.doi.org/10.1029/JB085iB02p00925.

Kendall, M., S. Maxwell, G. Foulger, L. Eisner, and Z. Lawrence, 2011, Microseismicity: Beyond dots in a box — Introduction: Geophysics, **76**, no. 6, WC1–WC3, http://dx.doi.org/10.1190/geo-2011-1114-SPSEIN.1.

Maxwell, S., 2010, Microseismic: Growth born from success: The Leading Edge, **29**, no. 3, 338–343, http://dx.doi.org/10.1190/1.3353732.

Maxwell, S. C., and C. L. Cipolla, 2011, What does microseismicity tell us about hydraulic fracturing?: Annual Technical Conference and Exhibition, SPE, Paper SPE 146932-M, http://dx.doi.org/10.2118/146932-MS.

Toksöz, M., D. Johnston, and A. Timur, 1979, Attenuation of seismic waves in dry and saturated rocks: I: Laboratory measurements: Geophysics, **44**, no. 4, 681–690, http://dx.doi.org/10.1190/1.1440969.

Acknowledgments

This work is funded by RPSEA-GTI Project 09122-04, RPSEA Project 09122-32, and the Penn State University Appalachian Basin Black Shale Group. We would like to thank Charles Ammon, Andy Nyblade, Rongmao Zhou, Guolong Su, Mike Mueller, Shawn Maxwell, Leo Eisner, Xiaofan Hu, John O'Donnell, and Erica Emry for many helpful discussions about microseismic and seismology. We would also like to thank Jon Olson for helpful reviews. We are grateful to Range Resources, Schlumberger, Microseismic Inc., and Gas Technology Institute for supplying the data.

Corresponding author: tanyunhui@gmail.com